Detection of ocean wave groupiness from spaceborne synthetic aperture radar

J. C. Nieto Borge, S. Lehner, A. Niedermeier and J. Schulz-Stellenfleth
Remote Sensing Technology Institute (IMF), German Aerospace Center (DLR), Wessling, Germany

Received 27 January 2004; revised 15 April 2004; accepted 6 May 2004; published 1 July 2004.

[1] In recent years a number of remote sensing techniques capable to provide two-dimensional information of the sea surface have been applied to describe sea states. This information is obtained from the estimation of the directional wave number spectrum. However, the wave number spectrum is not sufficient for a complete description of sea states. The analysis of some phenomena such as wave grouping, detection of individual waves, maximum wave heights, etc., needs a complementary study, which has been carried out historically in the temporal domain from buoy records. In two dimensions (e.g., the spatial domain), the complementary analysis of those phenomena can be carried out in the spatial domain rather than the temporal domain. In this work, two methods to analyze wave groupiness in the spatial domain from sea surface images are presented: The first method is based on the two-dimensional generalization of the Smoothed Instantaneous Wave Energy History (SIWEH) function, which had been originally developed to analyze wave groupiness for wave elevation time series. The second method uses the estimation of the wave envelope in two dimensions to extract wave grouping parameters. Assuming that the wave fields are Gaussian stochastic processes, both methods are applied to ERS-2 synthetic aperture radar (SAR) and ENVISAT advanced SAR (ASAR) images of the sea surface, where only cases with almost range traveling waves are considered in order to avoid strong nonlinearities in the SAR imaging mechanisms. The obtained results shown that spaceborne SAR can be used to extract wave grouping information on global scale. *INDEX TERMS:* 4275 Oceanography: General: Remote sensing and electromagnetic processes (0689); 4560 Oceanography: Physical: Surface waves and tides (1255); 4594 Oceanography: Physical: Instruments and techniques; *KEYWORDS:* SAR, wave grouping, surface waves

Citation: Nieto Borge, J. C., S. Lehner, A. Niedermeier, and J. Schulz-Stellenfleth (2004), Detection of ocean wave groupiness from spaceborne synthetic aperture radar, *J. Geophys. Res.*, *109*, C07005, doi:10.1029/2004JC002298.

1. Introduction

[2] It is well known that ocean gravity waves form wave groups [*Rice*, 1974; *Longuet-Higgins*, 1984; *Ochi*, 1998; *Goda*, 2000]. These groups are observed as sequences of high waves with nearly equal periods, or wavelengths. Wave groups are often responsible for serious damages to marine systems (i.e., ships, off and onshore structures, etc.) when the period of the individual waves in the group are close to the resonance period of the system. Traditionally, wave groups have been studied in the temporal domain (i.e., one dimension) by using buoy records [*Hamilton et al.*, 1979; *Donelan et al.*, 1996]. From these buoy records, time-dependent group properties can be derived at a fixed location of the ocean (e.g., the buoy deployment position). In recent years, alternative remote sensing methods to measure wave fields have been developed, such as video imaging systems [*Holland et al.*, 1997; *Piotrowski and Dugan*, 2002] and radar-based sensors [*Hasselmann et al.*, 1985; *Lehner et al.*, 2000; *Dankert et al.*, 2003]. In contrast to buoy records, which describe the vertical elevation of the sea surface as a function of time, remote sensing imaging techniques are able to describe wave fields in the spatial domain (i.e., two dimensions).

[3] This work presents methods to study wave groupiness features in the spatial domain, which are suitable to be applied to two-dimensional wave information obtained from remote sensing images of the sea surface. For wave elevation time series, the analysis of wave groups is carried out studying the slow temporal variations in the wave record. In a similar way, the analysis of wave groups in the spatial domain is carried out analyzing the long-scale variations of the wave elevation within the imaged sea surface. Two methods are used in this work to analyze wave groupiness: The two-dimensional extension of the Smoothed Instantaneous Wave Energy History (SIWEH) function derived originally by *Funke and Mansard* [1980] for wave elevation time series, and the analysis of wave groupiness from the estimation of the two-dimensional wave envelope. These two different methods are applied in this work to synthetic aperture radar (SAR)

0148-0227/04/2004JC002298$09.00

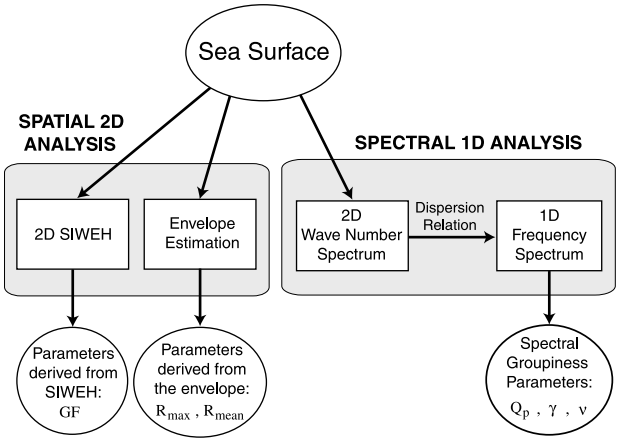

Figure 1. Scheme showing the different wave grouping analysis methods applied in this work.

images obtained by the European satellites ERS-2 and ENVISAT.

[4] The paper is structured as follows: In section 2 the theoretical assumptions used in this work to study wave grouping features in two dimensions is introduced. This section describes the two-dimensional extension of the SIWEH function, as well as the numerical technique used to estimate the two-dimensional wave envelope. As these methods are applied to SAR images, Section three summarizes the method to retrieve wave elevation maps from SAR images, these wave elevation maps are in the following used to extract wave grouping information. In section 4, the techniques are applied to ERS-2 and ENVISAT SAR images. Section 5 shows the results obtained from a large data set composed of more than 34,000 globally distributed ERS-2 SAR images. From the analysis of this large data set, scatterplots of wave grouping parameters derived from the spatial analysis versus some standard one-dimensional wave grouping parameters derived from the wave spectrum are presented. Figure 1 summarizes the application of all these different techniques. Finally, section 6 contains the conclusions of the paper.

2. Wave Grouping Description in Space and Time

2.1. Spectral Representation of Sea States

[5] For a finite area of the ocean, and assuming linear wave theory, the wave elevation η with respect to the mean sea level may be represented as a zero-mean Gaussian stochastic process depending on the sea surface coordinates $\mathbf{r} = (x, y)$. Under these assumptions, $\eta(\mathbf{r})$ can be regarded as the result of the superposition of different single components, each one determined by its amplitude, its wavelength, and its propagation direction. Hence $\eta(\mathbf{r})$ has the following spectral representation at fixed time (e.g., $t = 0$):

$$\eta(\mathbf{r}) = \sum_n a_n \cos(\mathbf{k}_n \cdot \mathbf{r} + \varphi_n), \tag{1}$$

where a_n, $\mathbf{k}_n = (k_{x_n}, k_{y_n})$, and φ_n are the amplitude, the wave number, and phase of each nth-wave component, respectively. The phases φ_n are usually considered as uniform distributed random variables in the interval $[-\pi, \pi)$.

[6] The variance σ_η^2 of the wave elevation is derived from the wave amplitudes as

$$\sigma_\eta^2 = \frac{1}{2}\sum_n a_n^2. \tag{2}$$

The variance σ_η^2 is proportional to the wave energy of waves coming from all the directions, and including all wavelengths, which form the wave elevation field described by equation (1).

2.2. Wave Group Determination in Two Dimensions From the Local Wave Energy

[7] As wave grouping is responsible for wave energy propagation, the spatial evolution of the potential energy of gravity waves is related to the distribution of wave groups in space. In addition, the potential wave energy per unit of area E_p is proportional to the squared value of the wave elevation η^2 [*Komen et al.*, 1994]. Therefore, taking into account the spectral representation of the wave elevation given by equation (1), E_p is given by

$$E_p(\mathbf{r}) \propto \eta^2(\mathbf{r}) = \frac{1}{2}\left[G^2(\mathbf{r}) + P^2(\mathbf{r})\right], \tag{3}$$

where $G^2(\mathbf{r})$ and $P^2(\mathbf{r})$ are the so-called group train and the pulse train, respectively [*Gran*, 1992; *Trulsen*, 2000; *Trulsen and Stansberg*, 2001]. The functions G^2 and P^2 are given by

$$G^2(\mathbf{r}) = \sum_m \sum_n a_m a_n \cos[(\mathbf{k}_m - \mathbf{k}_n)\cdot\mathbf{r} + (\varphi_m - \varphi_n)] \tag{4}$$

$$P^2(\mathbf{r}) = \sum_m \sum_n a_m a_n \cos[(\mathbf{k}_m + \mathbf{k}_n)\cdot\mathbf{r} + (\varphi_m + \varphi_n)], \tag{5}$$

where $1 \le m, n < \infty$.

[8] The long-scale spatial variabilities of $E_p(\mathbf{r})$ are explained by the group train $G^2(\mathbf{r})$, whereas $P^2(\mathbf{r})$ is related to the short-scale spatial variabilities of $E_p(\mathbf{r})$. Assuming that the wave components are statistically independent, the spatial averages of $G^2(\mathbf{r})$ and $P^2(\mathbf{r})$ are

$$\overline{G^2(\mathbf{r})} = \sum_n a_n^2 = 2\sigma_\eta^2, \quad \overline{P^2(\mathbf{r})} = 0. \tag{6}$$

Therefore, under the theoretical assumptions described above, the group train contains the information about the propagation of wave energy density per unit of area.

[9] Taking into account that the propagation of the wave energy is connected with the wave groupiness, *Funke and Mansard* [1980] introduced the SIWEH function to analyze wave groupiness features from wave elevation time series. A two-dimensional extension of the SIWEH function $E(\mathbf{r})$ can be defined as

$$E(\mathbf{r}) = \int_{\mathcal{A}} \left[\eta^2(\mathbf{r} - \mathbf{r}') - \overline{\eta^2}\right] W(\mathbf{r}') d^2 r', \tag{7}$$

where the integration domain $\mathcal{A}$ is the two-dimensional set defined by the finite area of the sea surface where the wave

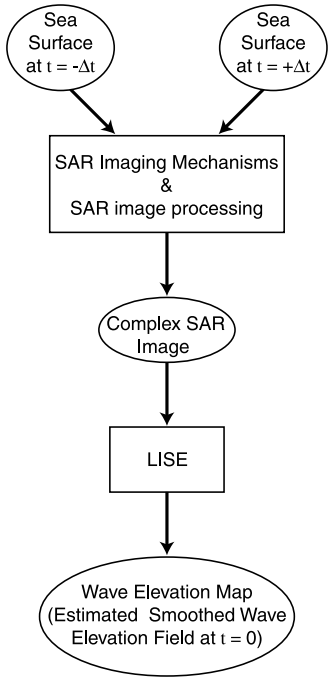

Figure 2. Scheme illustrating the application of the LISE method.

field can be considered statistically homogeneous. For simplicity, and due to the fact that all the techniques described in this work are applied to SAR images, $\mathcal{A}$ is considered as a rectangular set $\mathcal{A} \equiv [-L_x/2, L_x/2) \times [-L_y/2, L_y/2)$, which has a total area given by L_xL_y. For open sea conditions, typical values of L_x and L_y are about 10 km (e.g., assuming homogeneity is acceptable because SAR images used are approximately 5×10 km^2). In equation (7), the function $W(\mathbf{r}')$ is a two-dimensional Barlett window, which is used to filter out the spectral components related with the pulse train $P^2(\mathbf{r})$. Extending the theory behind the SIWEH function to two dimensions, the spectral cut-off variables used in the filter $W(\mathbf{r}')$ are given by the peak wave number $\mathbf{k}_p$. Hence equation (7) can be understood as an estimation of the group train $G^2(\mathbf{r})$, where the mean value of η^2 ($\overline{\eta^2} = \sigma_\eta^2$) has been subtracted.

[10] From the two-dimensional SIWEH function given by equation (7), the so-called groupiness factor *GF* is defined as

$$GF = \frac{1}{\sigma_\eta^2}\sqrt{\frac{1}{L_xL_y}\int_{\mathcal{A}} E(\mathbf{r})d^2r}. \tag{8}$$

The values of *GF* increase as the wave groupiness is higher.

2.3. Group Detection From the Wave Envelope in Two Dimensions

[11] An alternative way to detect the wave groupiness features is to use the wave envelope [*Longuet-Higgins*, 1984]. The wave envelope is defined from equation (1) by using the so-called complex signal ζ,

$$\zeta(\mathbf{r}) = \sum_n a_n e^{i(\mathbf{k}_n\cdot\mathbf{r}+\varphi_n)} = \eta(\mathbf{r}) + i\,\hat{\eta}(\mathbf{r}). \tag{9}$$

The complex signal ζ can be factored as the product of a local envelope $\rho(\mathbf{r})$ and the complex exponential of a local phase $\phi(\mathbf{r})$,

$$\zeta(\mathbf{r}) = \rho(\mathbf{r})e^{i\phi(\mathbf{r})}, \tag{10}$$

which implies $\eta(\mathbf{r}) = \rho(\mathbf{r})\cos[\phi(\mathbf{r})]$. Taking into account equations (3), (9), and (10), the squared wave envelope can be expressed as

$$\rho^2(\mathbf{r}) = \eta^2(\mathbf{r}) + \hat{\eta}^2(\mathbf{r}) = \frac{1}{2}\left[G^2(\mathbf{r}) + \hat{G}^2(\mathbf{r})\right], \tag{11}$$

where $\hat{G}^2$ is the group train of the imaginary part $\hat{\eta}$ of the complex signal. From equation (11), the spatial average of $\rho^2(\mathbf{r})$ is derived as $\overline{\rho^2} = 2\sigma_\eta^2$, which shows the connection between the wave envelope and the wave energy.

2.3.1. Probability Density Distribution of the Envelope Process

[12] Assuming that the wave elevation field is Gaussian distributed, the complex signal $\zeta(\mathbf{r})$ is a circular Gaussian process. Then the probability density function (PDF) of the envelope process follows a Rayleigh distribution [*Rice*, 1945; *Longuet-Higgins*, 1952; *Ochi*, 1998]. Assuming that the wave elevation $\eta(\mathbf{r})$ is a narrow-banded process, the probability that the maxima of $\eta(\mathbf{r})$ are located elsewhere than the wave crests is small. Hence ρ is strongly correlated with the amplitudes of the individual wave heights. In addition, for narrow-banded processes, there is a statistical symmetry for crests and troughs. Hence the wave height H can be derived from the wave envelope as $H = 2\rho$. Therefore, for narrow-banded processes, the wave height H is Rayleigh distributed [*Longuet-Higgins*, 1952; *Ochi*, 1998]. For those wave fields, which cannot be described as narrow-banded processes, the wave profile presents two or more local maxima and minima for one single wave cycle. In those cases a unique wave envelope cannot be defined properly [*Ochi*, 1998], and the wave height cannot be regarded as twice the envelope. Then it may be more appropriate to consider two statistically independent envelopes separated by one-half of the average wavelength. The narrow-band approach is used in further sections of this paper to estimate two-dimensional wave groupiness parameters from the wave envelope.

2.3.2. Numerical Estimation of the Wave Envelope in Two Dimensions

[13] In the one-dimensional analysis (i.e., wave elevation time series) the time-dependent envelope $\rho(t)$ can be estimated using the Hilbert transform [*Longuet-Higgins*, 1984],

$$\hat{\eta}(t) = \mathsf{P}\left\{\frac{1}{\pi}\int_{\mathbb{R}}\frac{\eta(\tau)}{t-\tau}d\tau\right\}, \tag{12}$$

where P denotes Cauchy's principle value. The instantaneous envelope is estimated as $\rho(t) = \sqrt{\eta^2(t) + \hat{\eta}^2(t)}$. For a higher number of dimensions (e.g., the spatial domain), a unique extension of equation (12) does not exist. In the wave grouping analysis derived from temporal sequences of marine radar images [*Dankert et al.*, 2003], the estimation of the two-dimensional envelope is reduced to a one-dimensional analysis in the frequency domain using

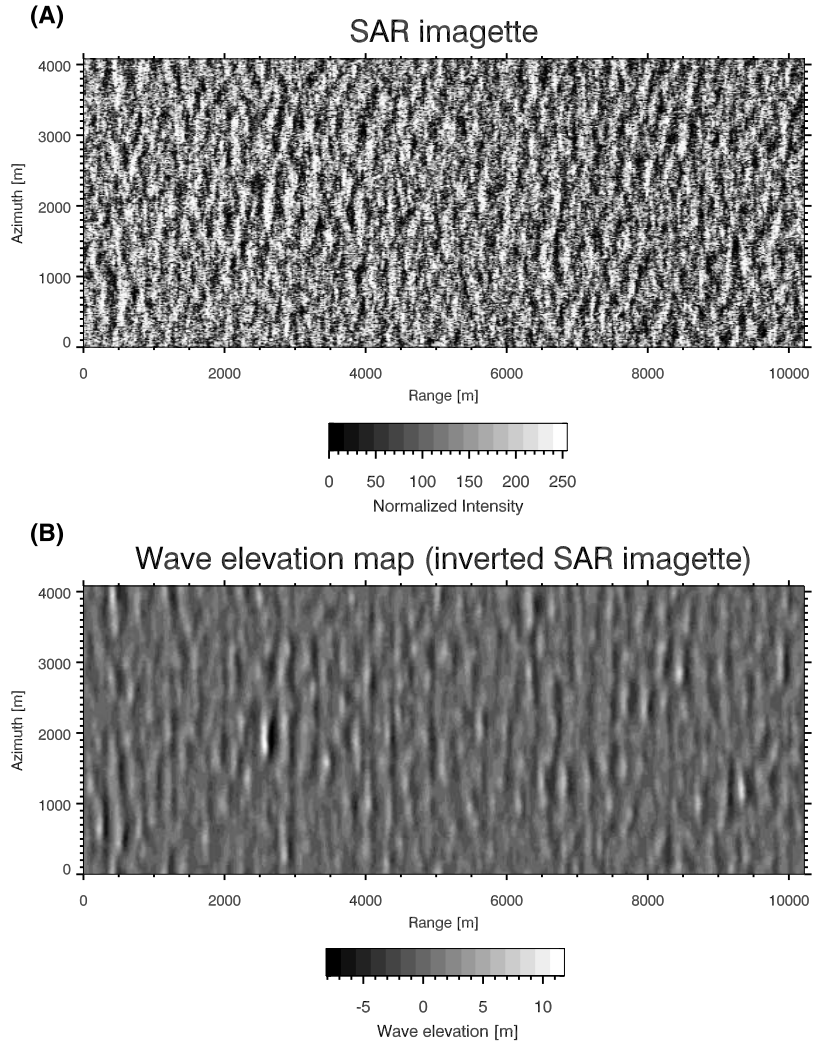

Figure 3. (a) Original ERS-2 wave mode image and (b) its corresponding wave elevation map, derived from the LISE method. The SAR measurement was taken by the ESA satellite ERS-2 in wave mode on 30 August 1996 at 2251:17 UTC. The image location is 44.6°S and 7.1°E.

the dispersion relation for linear gravity waves (see Appendix A). As this work uses satellite SAR images of the sea surface, a more natural domain to describe wave groupiness in two dimensions is the spatial domain itself, which permits us to avoid additional assumptions on the dispersion relation. For this approach, a two-dimensional generalization of the Hilbert transform has to be used. Several generalizations of the Hilbert transform for the multidimensional case can be found in the literature [*Stark*, 1971; *Bülow and Sommer*, 2001]. This work uses the *n*-dimensional definition of the Hilbert transform given by *Stark* [1971], which is known as Total Hilbert Transform (THT). For the two-dimensional case, the THT is defined as

$$\hat{\eta}_t(\mathbf{r}) = \mathrm{P}\left\{\frac{1}{\pi^2}\int_{\mathbb{R}^2}\frac{\eta(\lambda_x,\lambda_y)}{(x-\lambda_x)(y-\lambda_y)}d\lambda_x d\lambda_y\right\}. \qquad (13)$$

The THT estimation of the local envelope is then given by

$$\rho_t(\mathbf{r}) = \sqrt{\eta^2(\mathbf{r}) + \hat{\eta}_t^2(\mathbf{r})}. \qquad (14)$$

As it is described in the following section, the local envelope $\rho_t(\mathbf{r})$ given by equation (14) permits us to derive wave grouping parameters in two dimensions.

2.3.3. Wave Grouping Detection in Two Dimensions From the Local Envelope

[14] Taking into account that the wave height can be regarded as twice the wave envelope for narrow-banded wave fields (see section 2.3.1), a method to analyze wave groupiness features is to generalize the concept of a run used in time series analysis [*Goda*, 2000] to higher dimensions. In one dimension (e.g., wave elevation time series) a run is defined as the number of consecutive waves with wave heights higher than a specified threshold height H_0 [*Goda*, 2000]. Hence, in two dimensions a run area can be defined by the region of the sea surface where there are contiguous waves higher than a given threshold height H_0. The areas of each detected run, as well as the spatial distribution of them in the oceanic area of study, provide information about the two-dimensional wave groupiness features of the sea state.

[15] Taking into account equation (11), wave groupiness is described by the long local spatial variabilities of the

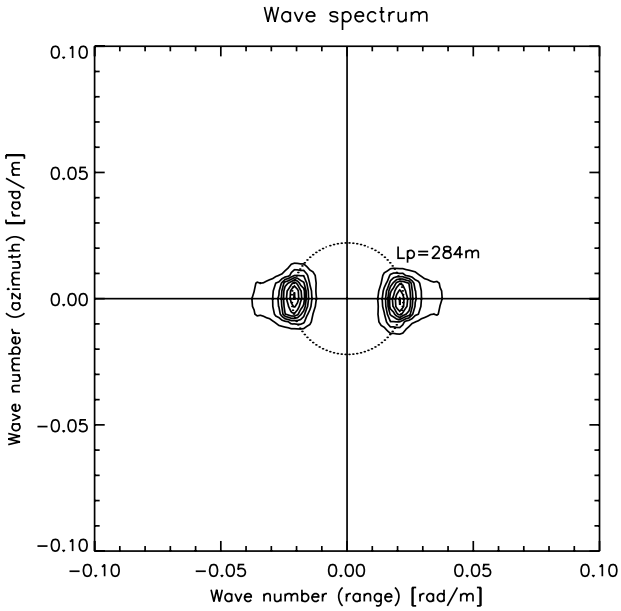

Figure 4. Wave number spectrum computed from the inverted wave elevation map shown in Figure 3. The significant wave height is H_s = 6.9 m. The circle indicates the peak wave number ($k = k_p = 2\pi/L_p$).

wave envelope, which correspond to the group train. Hence the wave envelope has to contain only spectral components defined by the second-order difference of wave number components ($\mathbf{k}_m - \mathbf{k}_n$) of the wave field $\eta(\mathbf{r})$. The envelope estimation ρ_t obtained from the two-dimensional THT (see equation (14)) introduces additional spectral components depending on the second-order summation ($\mathbf{k}_m + \mathbf{k}_n$) of wave number components. These summation components should be removed in order to filter the short local spatial variabilities of the envelope estimation given by equation (14). In addition, for the study of the group properties, only the dominant waves have to be taken into account [*Longuet-Higgins*, 1986]. One approach is to apply a band-pass filter to remove the summation components introduced by the two-dimensional THT [*Nieto Borge et al.*, 2003]. Therefore a smoothed envelope $\tilde{\rho}_t(\mathbf{r})$ is obtained. From $\tilde{\rho}_t(\mathbf{r})$, the two-dimensional run areas are then defined as the sea surface zones where $2\tilde{\rho}_t(\mathbf{r})$ is higher than the specified threshold height H_0. Once the run areas are identified, wave groupiness statistical analysis in space can be carried out. The statistical run area parameters extracted from each wave elevation field in this work are: the mean run area R_{mean}, and the area of the largest run $R_{\max}$ of each SAR image.

3. Estimation of Sea Surface Elevation From Complex SAR Data

[16] All the methods described in the previous section are applied to the wave elevation field $\eta(\mathbf{r})$. However, the analysis of SAR measurements of a sea surface provides intensity images $I(\mathbf{r})$ rather than wave elevation fields $\eta(\mathbf{r})$. The numerical value of each pixel in a SAR image $I(\mathbf{r})$ depends on how the sea surface backscatters the radar signal. The backscatter phenomenon is commonly described as a combination of many factors, such as the orbital motion of the water particles, wave tilting, roughness of the sea surface due to the local wind, etc. [*Alpers et al.*, 1981; *Hasselmann and Hasselmann*, 1991; *Krogstad*, 1992]. To determine the wave elevation for each position in the image $\eta(\mathbf{r})$, it is necessary to invert the original SAR intensity image $I(\mathbf{r})$ considering all known SAR imaging mechanisms. A single SAR image of a sea surface elevation field depends on the wave motion and the wave propagation directions. In particular, a single SAR intensity image is in general not sufficient to estimate the respective elevation field. Taking this idea into account, a recent technique to derive wave elevation maps from SAR complex images using a multilook technique has been developed by *Schulz-Stellenfleth and Lehner* [2004]. This inversion method is known as LISE (Quasilinear Inversion of Sea Surface Elevation Fields). Figure 2 shows a scheme illustrating the application of the LISE method. LISE is based on the spectral representation of the ocean wave field

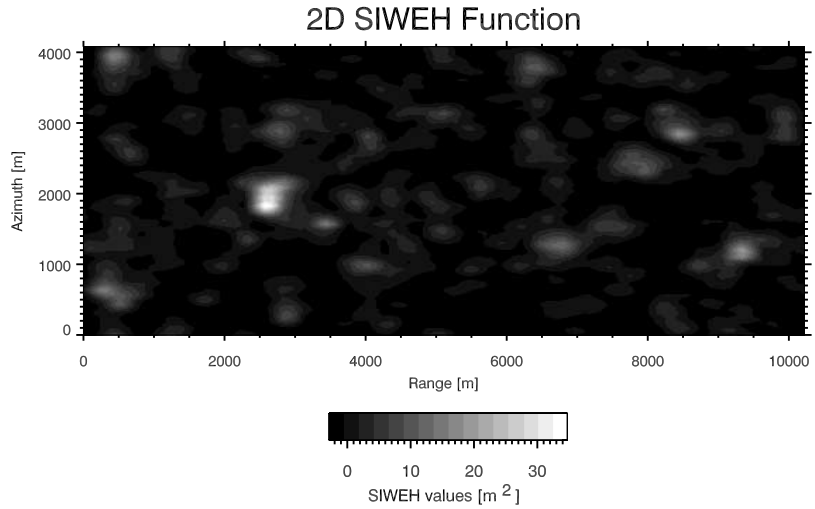

Figure 5. Two-dimensional SIWEH function (see equation (7)) derived from the wave elevation map shown in Figure 3.

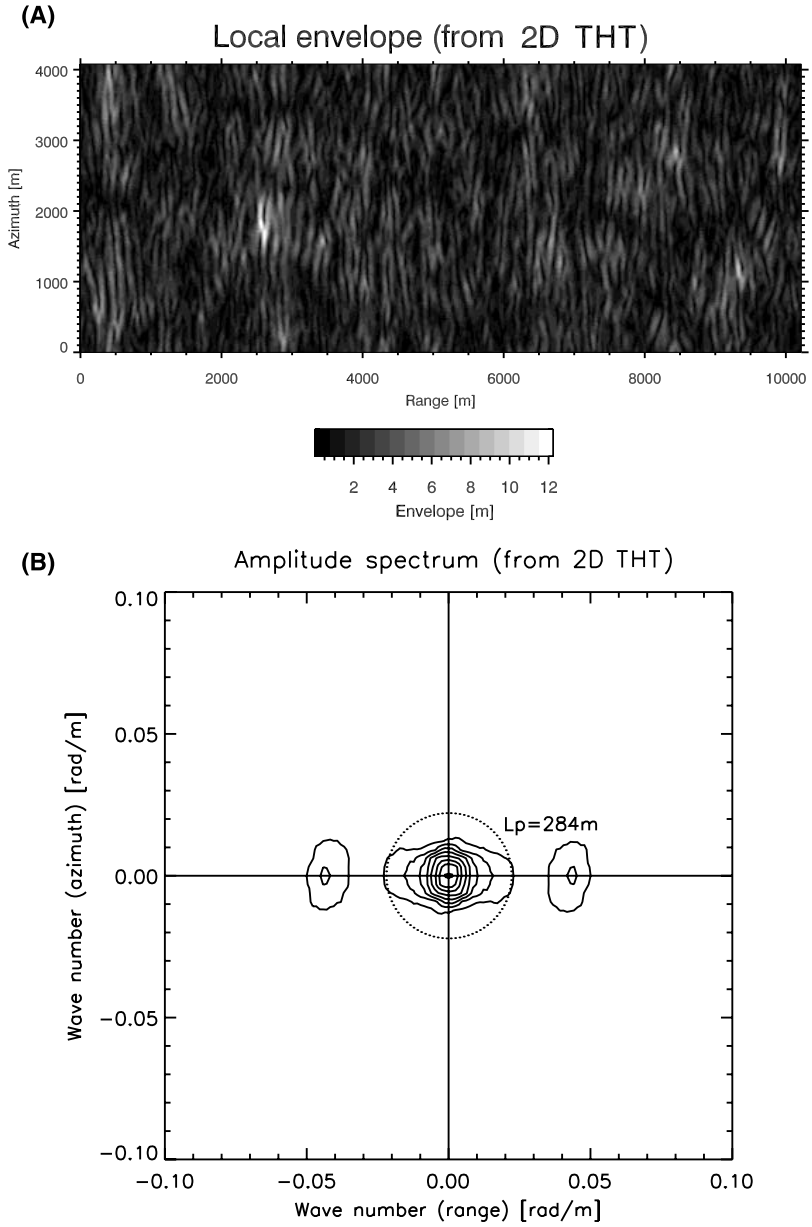

Figure 6. (a) Two-dimensional envelope $\rho_t(\mathbf{r})$ (see Equation 14) derived from the two-dimensional THT of the wave elevation map shown in Figure 3. (b) Corresponding spectral density of $\rho_t(\mathbf{r})$. The dotted line indicates the circle $k = k_p = 2\pi/L_p$.

$\eta(\mathbf{r})$, making use of two consecutive normalized SAR intensity looks $\mathcal{I}^{\pm}(\mathbf{r})$, which are separated by a time $2\Delta t$ in the order of half second. The two looks $\mathcal{I}^{\pm}(\mathbf{r})$ are related to the wave elevation field by

$$\mathcal{I}^{\pm}(\mathbf{r}) \equiv \frac{I^{\pm}(\mathbf{r}) - \langle I^{\pm} \rangle}{\langle I^{\pm} \rangle} = \mathrm{Re}\left[\sum_n a_n T_n e^{i(\mathbf{k}_n \cdot \mathbf{r} \pm 2\pi f_n \Delta t + \varphi_n)}\right], \quad (15)$$

where a quasilinear approximation of the SAR imaging model is used with a transfer function T_n [*Hasselmann et al.*, 1985; *Hasselmann and Hasselmann*, 1991], which includes the main SAR modulation Mechanisms as follows: (1) real aperture radar modulations: hydrodynamic modulation, tilt modulation, and range bunching; and (2) synthetic aperture radar modulations: velocity bunching.

[17] Inverting equation (15), the amplitudes a_n and phases φ_n of the imaged waves are determined. Hence the estimated wave elevation field $\eta(\mathbf{r})$ (called in this paper wave elevation map) can be calculated for the central time $t = 0$.

[18] The method described by equation (15) is limited to those waves imaged by spaceborne SAR (i.e., wavelengths longer than 100 m, or more depending on the wave propagation direction). Hence the synthesized wave elevation maps are in general narrow-banded processes. A detailed discussion about the range of validity of this technique, including those cases where wave fields present clear nonlinear features, is given by *Schulz-Stellenfleth and*

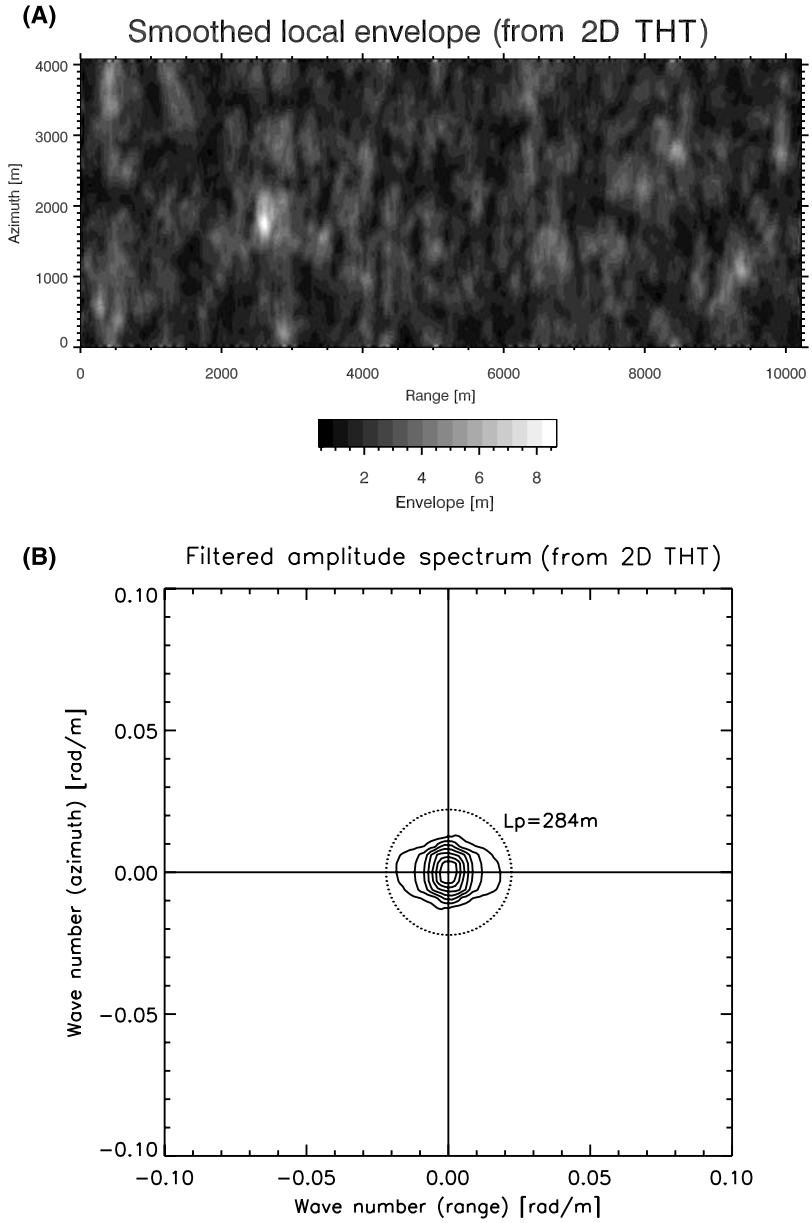

Figure 7. (a) Smoothed envelope $\tilde{\rho}_t(\mathbf{r})$. (b) Corresponding spectral density $\tilde{\rho}_t(\mathbf{r})$. The dotted line indicates the circle $k = k_p = 2\pi/L_p$.

Lehner [2004]. To select those measurements where the nonlinear SAR imaging effects are negligible, a degree of nonlinearity parameter C_{lin} [*Brüning et al.*, 1990] has been used in this work. For the case of a single wave system, C_{lin} can be derived as

$$C_{\text{lin}} \approx \sqrt{\frac{2\pi g}{L_p^3}} \frac{R}{v} \frac{H_s}{4} \sin\theta_R, \tag{16}$$

where L_p is the peak wavelength, θ_R is wave propagation direction relative to range, and R/v is the satellite range to velocity term, for ERS-2 $R/v \approx 111$ s. In our case, C_{lin} is estimated using the significant wave height H_s derived from the wave number spectrum $F(\mathbf{k})$ of the inverted wave elevation field. The linearization of the SAR imaging mechanisms is admissible for $C_{\text{lin}} < 0.7$, which is the case of long waves traveling close to range direction. The following section shows some examples of estimated wave elevation fields derived from the LISE scheme.

4. Examples of Wave Grouping Analysis Derived From Wave Elevation Maps

[19] In this section, examples of the wave group detection methods described previously are shown. The first example corresponds to an ERS-2 SAR wave mode image (scanned area about 10×5 km^2, with a spatial resolution of 16×20 m^2). Figure 3a shows the SAR intensity image, where a range traveling wave field can be seen. The corresponding inverted wave elevation map using the LISE scheme described in the previous section appears in Figure 3b. For this

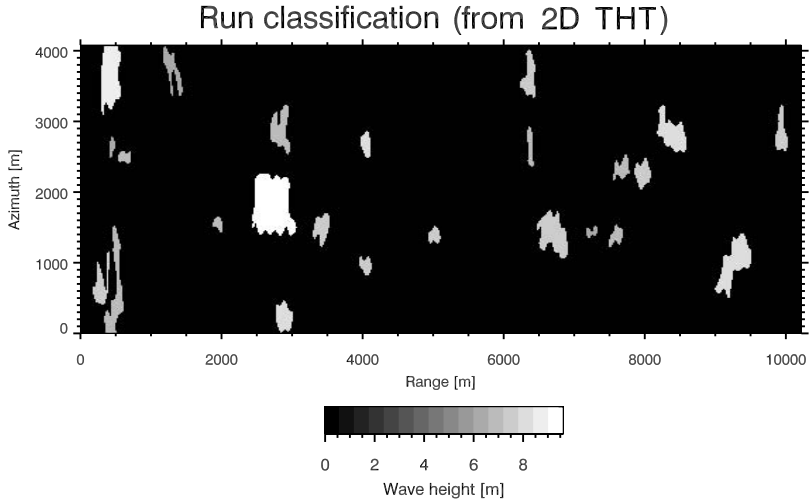

Figure 8. Classification of the two-dimensional runs from the smoothed envelope of Figure 7. The shading bar corresponds to the mean wave height of each run area.

SAR image, $C_{\text{lin}} = 0.087$. Figure 4 shows the wave number spectrum $F(\mathbf{k})$ derived from the two-dimensional Fourier transform of the inverted wave elevation field. Using this estimated wave elevation $\eta(\mathbf{r})$, the wave group analysis techniques described in the previous sections can be applied. Hence Figure 5 shows the corresponding two-dimensional SIWEH function. Furthermore, the local envelope $\rho_t(\mathbf{r})$ estimated from the two-dimensional THT of the wave elevation field in Figure 3b can be seen in Figure 6a. This estimation of the envelope contains both short and long local spatial variabilities, which are related, respectively, to the high and low wave number spectral components of $\rho_t(\mathbf{r})$ (see Figure 6b, where the two-dimensional spectral density of $\rho_t(\mathbf{r})$ is shown). After the application of the band-pass filter, as described in section 2.3.3, a smoothed wave envelope $\tilde{\rho}_t(\mathbf{r})$ is obtained. Figure 7 shows the smoothed envelope (Figure 7a) and its corresponding two-dimensional spectral density (Figure 7b), where the spectral components of higher wave numbers than the peak wave number k_p have been filtered.

[20] Figure 8 shows the run areas obtained after thresholding the smoothed envelope $\tilde{\rho}_t(\mathbf{r})$ multiplied by 2. The threshold height used is the significant wave height $H_0 = H_s$. The color table of the figure corresponds to the averaged wave height within each run area. It can be seen that the spatial distribution of the run areas in Figure 8 is similar to the structures given by the SIWEH function (see Figure 5).

[21] A second example of wave group detection on a SAR images can be seen in Figures 9–14, this measurement was taken by the ENVISAT advanced SAR (ASAR). The measurement shows an almost range traveling wave field. Figure 9a shows the normalized intensity wave mode image. The corresponding wave elevation map derived from the LISE scheme is shown in Figure 9b. Figure 10 shows the corresponding two-dimensional spectral density $F(\mathbf{k})$ of the wave elevation map. The significant wave height derived from $F(\mathbf{k})$ is $H_s = 5.1$ m and the spectral peak wavelength is $L_p = 223$ m. For this ASAR image, $C_{\text{lin}} = 0.06$. The corresponding two-dimensional SIWEH function is shown in Figure 11. In addition, the THT estimation of the wave envelope $\rho_t(\mathbf{r})$ and the smoothed envelope $\tilde{\rho}_t(\mathbf{r})$, as well as their related two-dimensional spectral densities, appear in Figures 12 and 13, respectively. The run areas are determined using the significant wave height as the threshold height in the same way as the previous example. These detected run areas are shown in Figure 14, where, like in the previous example, the color code corresponds to wave height averaged within each run area. Comparing the smoothed envelope $\tilde{\rho}_t(\mathbf{r})$ shown in Figure 13a with the SIWEH function in Figure 11, it can be seen that only the areas where SIWEH indicates high wave groupiness corresponding to those run areas with higher values of the averaged wave height. Hence, due to the fact that the two-dimensional SIWEH function is proportional to a smoothed squared wave elevation, some wave groupiness features relating to groups composed of not extremely high waves cannot be identified from the SIWEH function, and therefore the value of the groupiness factor GF is only affected by those groups of waves that contain high waves compared to the average wave elevation of the analyzed sea state.

[22] To take the advance of the global scale coverage of satellites, the techniques described in the previous sections are applied to analyze wave grouping in open ocean. The following section shows the obtained results.

5. Wave Group Statistics From Globally Distributed ERS-2 SAR Data Set

5.1. Description of the Data

[23] A data set consisting of 34,310 ERS-2 SAR wave mode images has been used to carry out the analysis of wave groups on a global scale. The data were taken by the ERS-2 satellite during September 1996 (late winter season in the Southern Hemisphere). Each SAR image has been processed from the original ERS-2 raw data by using the BSAR processor [*Breit et al.*, 1997; *Lehner et al.*, 1998] developed at the German Aerospace Center (DLR). A quality control check has been applied to reject all those ERS-2 SAR wave mode images containing sea ice for latitudes close to polar locations, and a homogeneity test

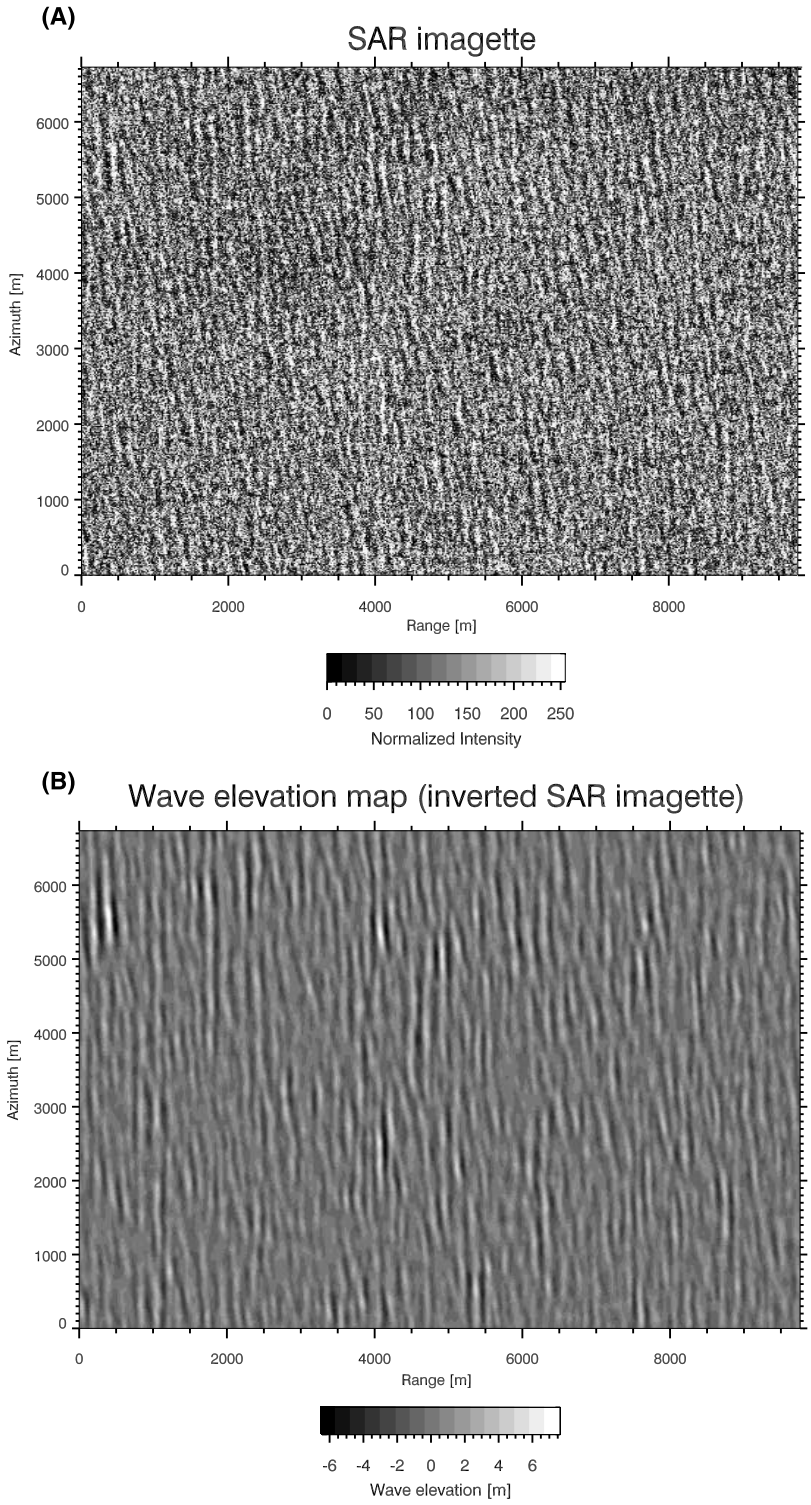

Figure 9. (a) Normalized intensity image and (b) its corresponding wave elevation map derived from the LISE method. The measurement was taken by the ENVISAT ASAR in wave mode on 9 July 2002 at 1925:17 UTC. The image location is 42.71°N and 136.96°W.

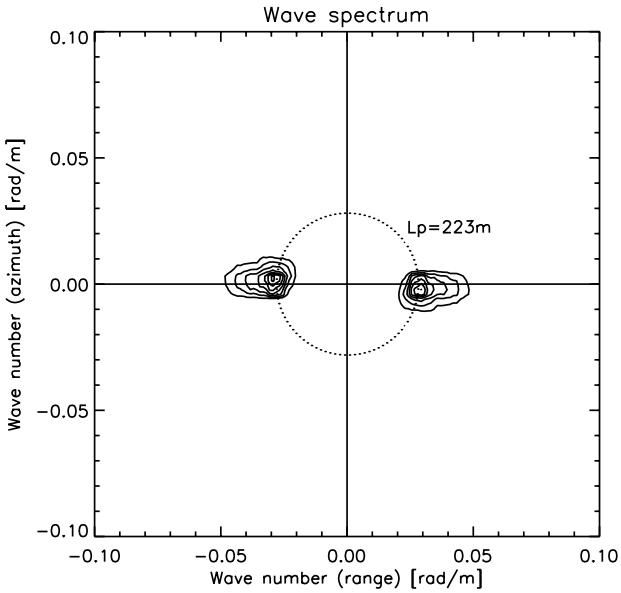

Figure 10. Wave number spectrum computed from the inverted wave elevation map shown in Figure 9. The significant wave height is H_s = 5.1 m. The circle indicates the peak wave number ($k = k_p = 2\pi/L_p$).

has been carried out to detect and reject all those SAR images presenting nonhomogeneous wave fields. Finally, the degree of nonlinearity parameter C_{lin} was calculated to detect strong nonlinear features in the SAR imagery. Only those cases where $C_{\text{lin}} < 0.7$ were taken into account. After the application of the quality control check mentioned above, 28% SAR wave mode images of the total data set were rejected.

5.2. Results of the Analysis of Globally Distributed Data

[24] For each ERS-2 SAR wave mode image, the LISE method was applied to derive the corresponding wave elevation map $\eta(\mathbf{r})$. Then the different techniques described in the previous sections were applied to extract wave grouping information for each SAR measurement. The goal of this work is to develop spatial domain techniques able to describe wave groupiness in two dimensions. Hence the results obtained from these techniques are compared to standard one-dimensional wave parameters in order to find out if the spatial domain techniques provide consistent information about wave groups. To compare the spatial and temporal evolution of wave fields, it is necessary to assume ergodicity for those wave fields. Hence the spatial domain wave grouping parameters can be compared to the one-dimensional ones. Taking into account the dispersion relation for linear gravity waves (see Appendix A), it is possible to derive one-dimensional wave grouping parameters from the wave number spectrum $F(\mathbf{k})$ of the wave elevation maps. The deep water approximation of the dispersion relation $f(k) = \sqrt{gk}/(2\pi)$ was used because the ERS-2 SAR measurements of the analyzed data set were taken over the open ocean. Three different one-dimensional sea state parameters are calculated: Wave correlation between consecutive wave heights γ, peakedness parameter Q_p, and spectral bandwidth ν (see Appendix A for the definition of these parameters). Figure 15 illustrates the dependence of those parameters obtained from the wave number spectra calculated for the wave elevation map

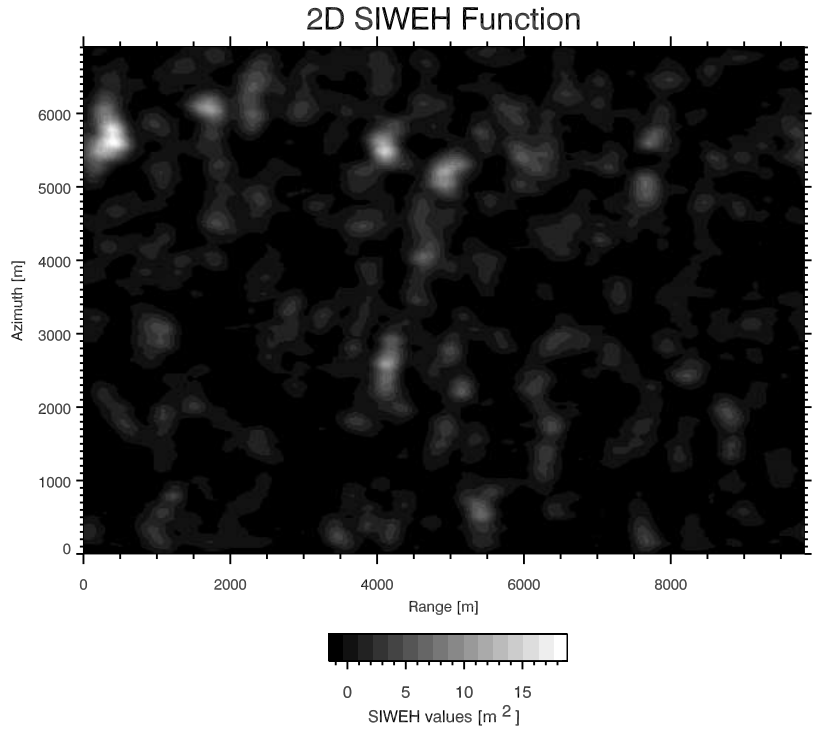

Figure 11. Two-dimensional SIWEH function (see equation (7)) derived from the wave elevation field shown in Figure 9b.

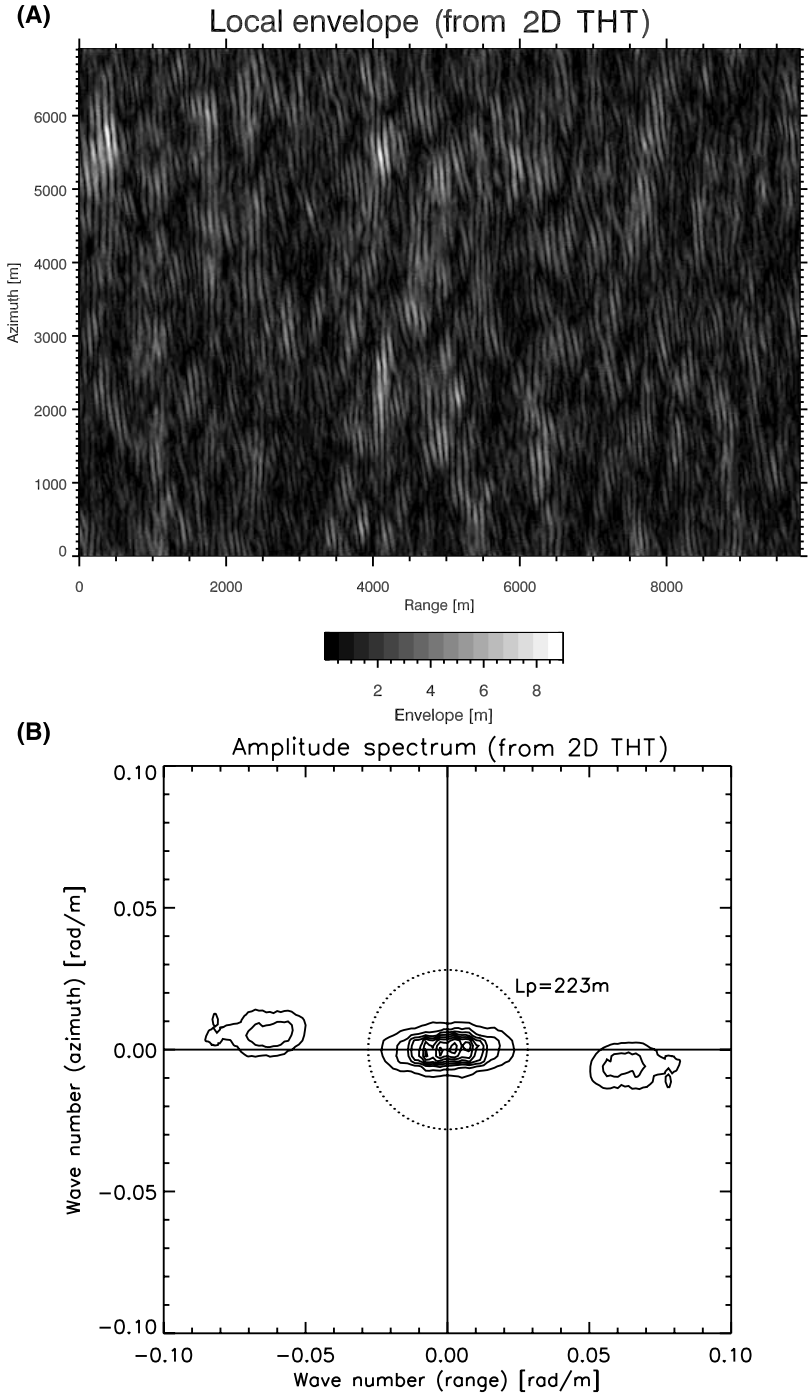

Figure 12. (a) Two-dimensional envelope $\rho_t(\mathbf{r})$ (see equation (14)) derived from the THT of the wave elevation map showed in Figure 9. (b) Corresponding spectral density of $\rho_t(\mathbf{r})$. The dotted line indicates the circle $k = k_p = 2\pi/L_p$.

derived from each ERS-2 image. Wave groupiness increases as consecutive wave heights are more correlated. Hence, as Figure 15 shows, when wave heights present higher correlation (high values of γ) the peakedness parameter Q_p presents higher values as well. In addition, both parameters present a decreasing dependence on the spectral bandwidth ν, which indicates that the wave groupiness increases for those cases where the wave spectrum is narrower. Figure 15 shows a high value of the correlation index (r = 0.874) between γ and Q_p. This high value of r is due to the long waves lengths (L > 100 m, approximately) in spaceborne SAR images. Not all the wave components are imaged by the spaceborne SAR, and the wave elevation maps derived from the LISE method are narrow-banded processes. For buoy records a higher scatter between Q_p and γ is expected [*Medina and Hudspeth*, 1990] because this measurements include the short wind waves, which are generally less correlated. Nevertheless, it can be seen in Figure 15 that

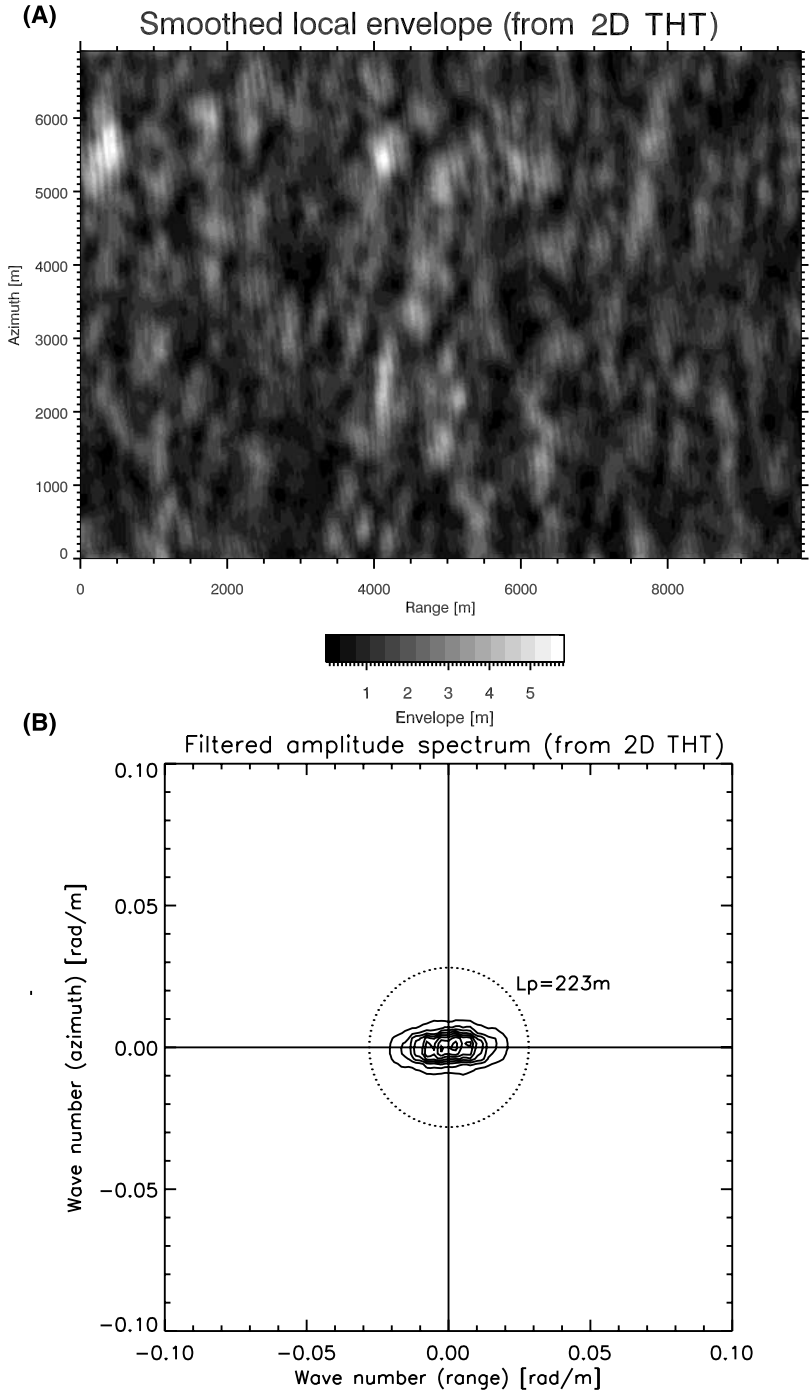

Figure 13. (a) Smoothed envelope $\tilde{\rho}_t(\mathbf{r})$. (b) Corresponding spectral density of $\tilde{\rho}_t(\mathbf{r})$. The dotted line indicates the circle $k = k_p = 2\pi/L_p$.

those measurements with a low correlation between consecutive wave heights present a high scatter of Q_p, which is consistent with those results obtained from wave elevation time series.

5.2.1. Comparisons Between the Groupiness Factor and the Run Areas

[25] Figure 16a shows the comparisons of the groupiness factor *GF* (see equation (8)) derived from the two-dimensional SIWEH function and the mean run area R_{mean} derived from the smoothed wave envelope. It can be seen that the probability of detecting larger areas of contiguous high waves increases for higher values of *GF*. An empirical exponential dependence of R_{mean} on *GF*, with a correlation value of 0.77, is found by using a least squares fit. In a similar way, Figure 16b shows the scatterplot of *GF* versus the largest run area R_{max} found for each ERS-2 wave elevation map. In both plots the color coding refers to the spectral bandwidth ν. It can be seen that there is a dependence between these three parameters: When *GF* increases, the run areas increase

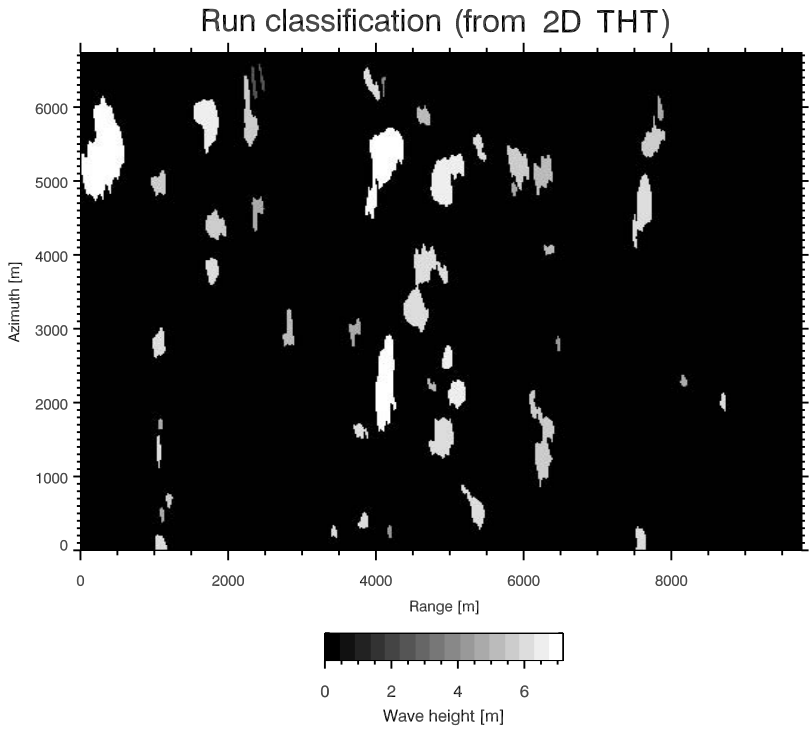

Figure 14. Classification of the two-dimensional runs from the smoothed envelope in Figure 7.

as well. In addition, when the spectral bandwidth decreases, the probability of obtaining a higher wave grouping features in the spatial domain increases. In general, as the example of Figure 11 shows, and due to the fact that the two-dimensional SIWEH function is derived from the square of the wave elevation, the wave groupiness information derived from SIWEH, and therefore from the groupiness factor *GF*, is mainly influenced by those areas of the sea surface where the extreme waves are located. Hence there are some run areas that are not properly detected by SIWEH because the waves within are not extremely high. In general, the wave groupiness parameters derived from the envelope (see Figure 1) are more reliable to study wave grouping in two dimensions because the wave envelope is derived taking into account all the long local spatial variability elevations of the sea surface. As a result of this limitation of the SIWEH function, it can be seen in Figure 16 that the correlation of the spectral bandwidth ν with *GF* is not as strong as with other spectral parameters (see section 5.2.2).

[26] As all the SAR images analyzed in this work cover the same oceanic area (10×5 km^2), the run areas are proportional to the estimation of the probability of finding consecutive waves higher than a specified threshold height H_0 (in this case, $H_0 = H_s$). Analyzing the values of R_{mean} found from the data set used in this work, it can be seen that the values of R_{mean} are in most of the cases comparable to L_m^2. This result can be interpreted as there is a small probability of finding several consecutive waves in the open ocean with wave heights higher than H_s. In most of the cases, the two-dimensional runs contain one or two waves. Similar results are found for buoy records, where the number of waves within each run decreases as the threshold height H_0 increases [*Sorensen*, 1994; *Goda*, 2000]. For those buoy records, and when $H_0 = H_s$, most of the runs contained only one wave.

5.2.2. Comparisons Between the Run Areas and the Wave Groupiness Parameters Derived From the Frequency Spectrum

[27] Figure 17 shows the dependence found between the run areas (R_{mean} and R_{max}) and the peakedness parameter Q_p (see equation (A5)). The dots in these plots are given in a color coding referring to the values of the spectral band-

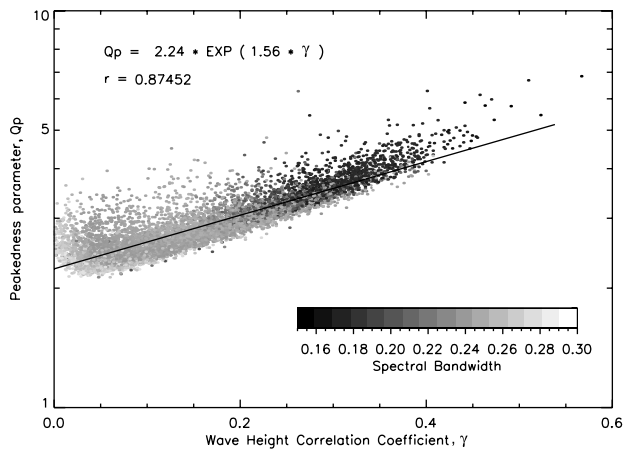

Figure 15. Wave height correlation coefficient γ versus peakedness parameter Q_p as a function of the spectral bandwidth ν (see equations (A3), (A5), and (A6), respectively). These parameters have been calculated from the wave number spectrum $F(\mathbf{k})$ derived from the Fourier decomposition of each wave elevation maps by applying the LISE method to the data set of globally distributed ERS-2 SAR wave mode images. See color version of this figure in the HTML.

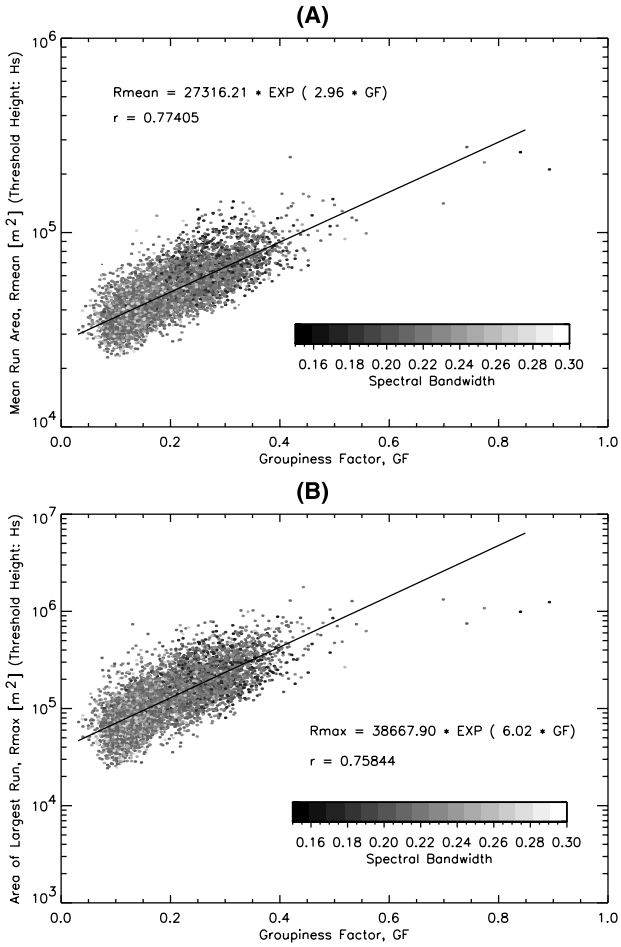

Figure 16. (a) Groupiness factor *GF* (see equation (8)) from the two-dimensional (2-D) SIWEH function versus the mean value of the run areas in each ERS-2 SAR wave mode image. (b) Groupiness factor *GF* from the 2-D SIWEH function versus the maximum value of the run areas in each ERS-2 SAR wave mode image. The used threshold height for run area computation is H_s. The color code corresponds to the spectral bandwidth ν derived from the spectrum. See color version of this figure in the HTML.

width ν. It can be seen that when the area of the two-dimensional runs is larger than the probability of finding a higher value of Q_p increases. In these cases the probability of finding a lower value of ν increases as well.

[28] The dependence between R_{mean} and R_{max} on a temporal domain parameter is more clear when the wave correlation γ is used (see Figure 18). The reason for this is that the estimation of γ is not as sensitive as Q_p to the frequency resolution in $S(f)$ [*Goda*, 2000]. Figure 18 has been color coded depending on the mean wavelength L_m, showing that wave groupiness features are more present for those sea states with longer waves.

5.2.3. Dependence Between the Mean Run Area and the Area of the Largest Run

[29] One of the studies that can be carried out from the data set used in this work is the estimation of the expected area of largest run R_{max} for a given mean run area R_{mean}. Figure 19a shows a power law dependence between R_{mean} and R_{max}, where the scatter increases as the values of both variables are higher. The dots in this plot are color coded depending on the value of the mean wavelength L_m. For the data set used in this work, the probability of finding larger run areas increases for those cases where the sea state consists of larger waves. Figure 19b shows the histogram of the random variable $R_{\text{max}}/R_{\text{mean}}$. The resulting histogram presents an exponential decay law for high values of $R_{\text{max}}/R_{\text{mean}}$. From this histogram, the expected value of R_{max} found for a given value of R_{mean} is estimated as 2.5 times R_{mean}. This expected value of R_{max} depends in general on the total number of waves within the imaged sea surface area. Hence, if the area of analysis is enlarged, higher values of R_{max} must be obtained. The value $R_{\text{max}}/R_{\text{mean}} \approx 2.5$ is an averaged expected value obtained from different sea states result of different meteorological conditions. A more detailed analysis can be carried out selecting different sea state situations, as well as consid-

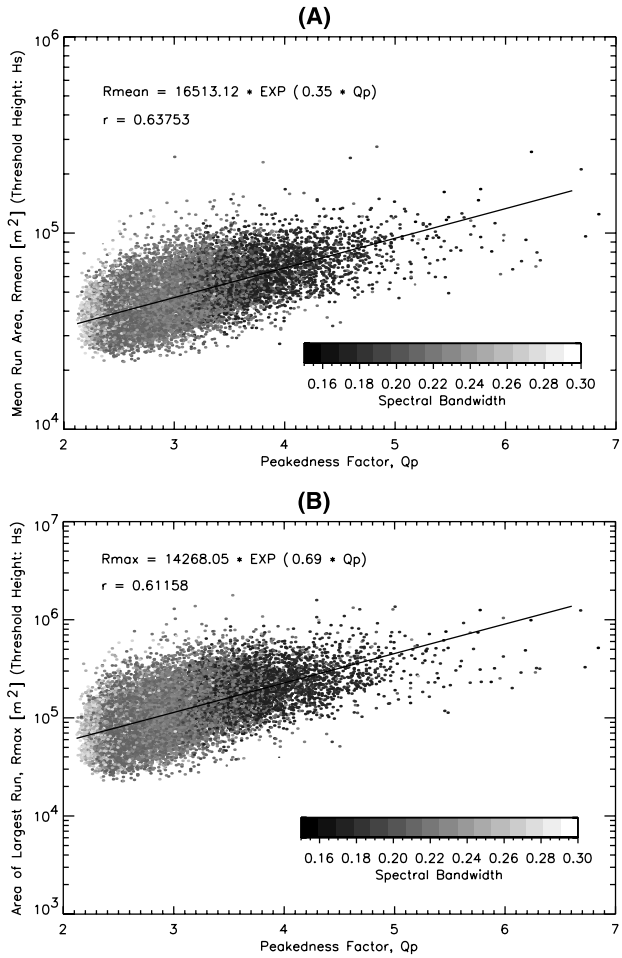

Figure 17. (a) Peakedness parameter Q_p versus the mean value of the run areas in each ERS-2 SAR wave mode image. (b) Peakedness parameter Q_p versus the maximum value of run areas in each ERS-2 SAR wave mode image. The used threshold height for run area computation is H_s. The color code corresponds to the spectral bandwidth ν derived from the spectrum. See color version of this figure in the HTML.

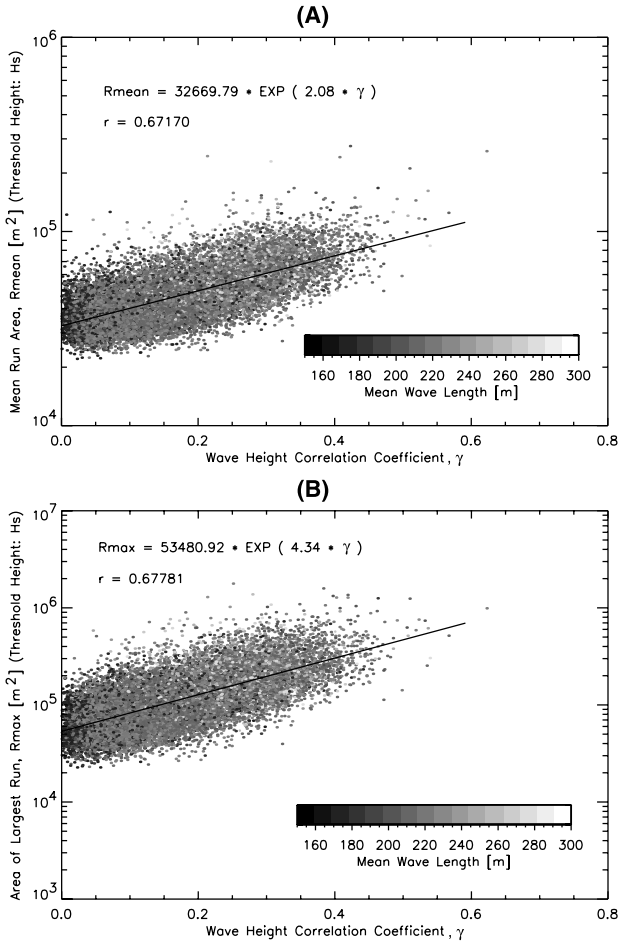

Figure 18. (a) Wave height correlation coefficient γ versus the mean value of the run areas in each ERS-2 SAR wave mode image. (b) Wave height correlation coefficient γ versus the maximum value of the run areas in each ERS-2 SAR wave mode image. The used threshold height for run area computation is H_s. See color version of this figure in the HTML.

ering the number of single waves within each two-dimensional run instead of the run areas.

6. Conclusions and Outlook

[30] Two different spatial domain techniques to analyze wave grouping in two dimensions have been presented. Assuming Gaussian wave fields, both methods are applied to images of the sea surface measured by remote sensing systems. For complex SAR images of the ocean, first an inversion scheme to extract the wave field information in the spatial domain from the radar image is used before wave grouping is analyzed. This inversion scheme assumes a quasilinear model of the SAR imaging mechanisms, which is a valid approximation for those cases where the wave propagation direction is close to the SAR range direction. The first wave grouping analysis method described in this work is based on a two-dimensional generalization of the SIWEH function. In the second method the estimation of the wave envelope derived from a two-dimensional Hilbert transform is used to detect those sea surface areas where consecutive waves that are higher than a given threshold height are present. In general, for those sea surface areas where consecutive waves are high compared to the average sea state, there is a good agreement between the spatial distribution of wave groups given by the SIWEH function and the spatial distribution of wave groups extracted from the wave envelope analysis. When the sea surface contains many areas with non-extremely high consecutive waves, the SIWEH function is not able to determine properly the wave groupiness features. Thus the method based on the wave envelope is more reliable to apply to any kind of sea surface, as well as for lower sea states.

[31] Using a data set of globally distributed ERS-2 SAR wave mode images, a comparison between the parameters extracted from these two methods defined in the spatial domain and common standard groupiness parameters derived from the one-dimensional wave spectrum has been carried out. The main difference between the calculation of the groupiness parameters defined in the spatial domain and the calculation of the groupiness parameters defined from the frequency spectrum is that for the derivation of second ones it is necessary to impose the dispersion relation as an additional assump-

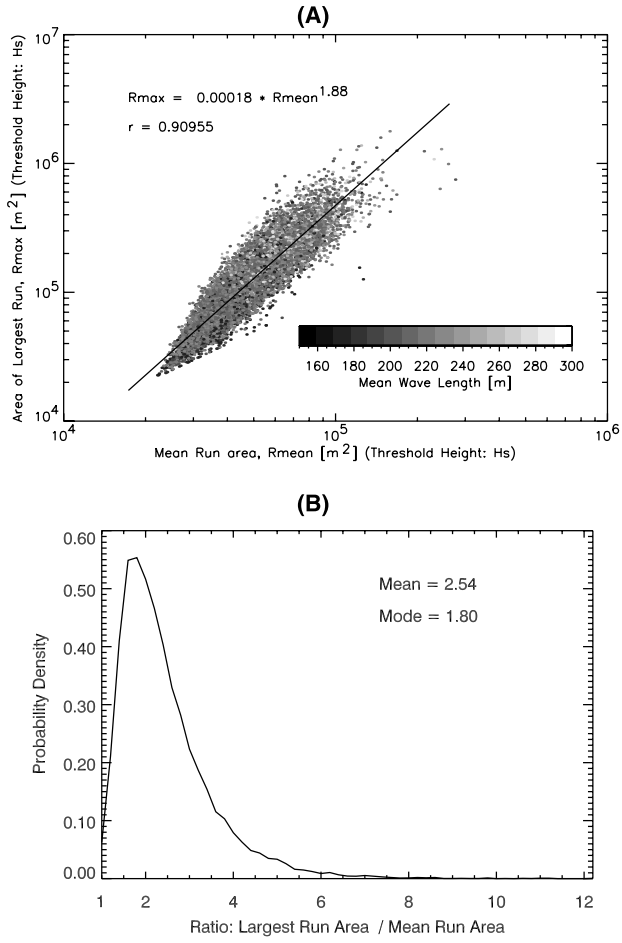

Figure 19. (a) Mean run area R_{mean} versus the area of the largest run R_{max} for each ERS-2 SAR wave mode image, and (b) histogram of the ratio R_{max}/R_{mean}. See color version of this figure in the HTML.

tion. Furthermore, similar to the way one-dimensional wave grouping analysis for wave elevation time series is normally carried out in the temporal domain rather than the spectral domain, the analysis of wave groups in two dimensions can be done by using spatial domain techniques, complementing and extending the information extracted from the wave spectrum. In particular, the identification of the mean and maximum sea surface areas where consecutive high waves travel together can be carried out. These areas can be compared with the size of offshore structures, such as oil platforms, in order to estimate if the extension of the structure can be completely covered by the larger wave groups. In this work, wave grouping areas larger than 1000×1000 m^2 have been detected in the Southern Hemisphere for late winter.

[32] From the results derived from the ERS-2 SAR data set, it can be concluded that SAR images are a reliable tool to detect and identify areas where waves are more grouped in open ocean and on a global scale. For future work, comparisons between the wave elevation maps derived from the inversion scheme and their corresponding two-dimensional wave grouping parameters with those obtained from in situ data have to be carried out. At this time, only 34,310 SAR images distributed along 27 days were used. This data set is still too small to carry out climate studies about wave groups in the open ocean for different geographical locations. Nowadays, more than 10 years of SAR raw data are available from different satellites. This huge amount of data will be a new source of information for a long-term analysis of the wave grouping phenomenon.

Appendix A: One-Dimensional Spectral Groupiness Parameters

[33] The analysis of wave groups has been traditionally carried out in the temporal domain from wave elevation time series measured by buoys. From those wave elevation time series, different parameters to describe the groupiness properties of consecutive waves in one dimension can be derived [*Medina and Hudspeth*, 1990]. All those parameters depend on the correlation between consecutive wave heights in the wave record. Some of those one-dimensional group parameters can be calculated from the frequency spectrum $S(f)$. For spatially dependent wave fields $\eta(\mathbf{r})$, the one-dimensional spectral parameters can be derived from the two-dimensional wave number spectrum $F(\mathbf{k})$ taking into account the dispersion relation for linear gravity waves,

$$f(k) = \frac{1}{2\pi}\sqrt{gk\tanh(kh)}, \tag{A1}$$

where $k = |\mathbf{k}|$, g is the acceleration of the gravity, and h is the water depth.

[34] Hence, for a given wave number spectrum $F(\mathbf{k})$, the corresponding one-dimensional frequency spectrum $S(f)$ is [*Nieto Borge et al.*, 1999]

$$S(f) = 4\pi \int_{-\pi}^{\pi} F(\mathbf{k}(k(f),\theta))\frac{k(f)}{c_g(f)}d\theta, \tag{A2}$$

where $k(f)$ is the inverse function of the dispersion relation (equation (A1)), $\theta = \tan^{-1}(k_y/k_x)$ is the wave propagation direction, and $c_g = 2\pi df/dk$ is the group velocity. The one-dimensional spectral groupiness parameters used in this work are wave height correlation coefficient γ, peakedness parameter Q_p, and spectral bandwidth ν, which are described in the following.

A1. Wave Height Correlation Coefficient γ

[35] Gravity waves are more grouped when the correlation between consecutive wave heights increases. Hence a reliable theory to analyze wave groups requires us to take into account the correlation coefficient between consecutive wave heights γ. For wave elevation time series, the theory was first introduced by *Kimura* [1980], and after re-presented by *Battjes and van Vledder* [1984] and *Longuet-Higgins* [1984], both of whom expressed γ as a function of the frequency spectrum $S(f)$. From the cited theory, the wave height correlation coefficient γ between two wave heights separated a time τ is given by [*Kimura*, 1980],

$$\gamma = \frac{\mathcal{E}(\kappa) - (1-\kappa^2)\mathcal{K}(\kappa)/2 - \pi/4}{1 - \pi/4}, \tag{A3}$$

where $\mathcal{E}(\kappa)$ and $\mathcal{K}(\kappa)$ are complete elliptic integrals of 1st and 2nd kind, respectively. The parameter κ in equation (A3) depends on the separation time τ. Here κ can be estimated for a characteristic time $\tau = T_e = m_0/m_1$ (where $m_0 = \sigma_\eta^2$, and m_1 are the zeroth and first spectral moments, respectively) by using the expression [*Longuet-Higgins*, 1984],

$$\kappa = \left|\frac{1}{m_0}\int_0^\infty S(f)e^{i2\pi f T_e}df\right|. \tag{A4}$$

A2. Peakedness Parameter Q_p

[36] This sea state parameter proposed by *Goda* [1970] depends on the spectral shape. Q_p varies from 1 to around 2 for wind waves and has values greater than 2 for swell. Q_p has also the capability to describe empirically the statistical features of consecutive wave heights, because Q_p presents higher values for those wave elevation records where waves are more grouped [*Ochi*, 1998; *Goda*, 2000]. Q_p is defined from the frequency spectrum $S(f)$ as

$$Q_p = \frac{2}{m_0^2}\int_0^\infty fS^2(f)df. \tag{A5}$$

The term $S^2(f)$ in equation (A5) is used to give more weight to those wave components with higher contribution to the total wave energy (e.g., wave components around the spectral peak). The numerical estimation of Q_p is very sensitive to the frequency resolution of $S(f)$. Though this problem occurs as well for the estimation of the parameter κ given by equation (A4), the numerical computation of κ (and therefore γ) is less sensitive than Q_p [*Goda*, 2000].

A3. Spectral Bandwidth ν

[37] Although ν is not a common wave grouping parameter, it is a well known fact that wave groupiness features are strongly correlated with the spectral bandwidth [*Goda*, 2000]. Hence wave groupiness is higher as the wave spectrum is narrower. In this work the spectral bandwidth

parameter ν defined by *Longuet-Higgins* [1984] is used, which indicates the degree of the spectral energy spreading over the frequency range. The parameter ν is defined as

$$\nu = \sqrt{\frac{m_2 m_0}{m_1^2} - 1}. \quad \text{(A6)}$$

This parameter varies from 0 to 1 from a very narrow to very broad spectrum, respectively. The frequency spectrum $S(f)$ is characterized as narrow when $\nu \ll 1$.

Notation

$\mathbf{r}$	sea surface coordinate vector, m.
t	time, s.
$\mathbf{k}$	wave number vector, rad/m.
θ	wave propagation direction, rad.
L	wavelength, m.
L_p	peak wavelength, m.
L_m	mean wavelength, m.
E_p	potential wave energy per unit of area, J.
H_s	significant wave height, m.
g	acceleration of the gravity, m/s^2.
h	water depth, m.
c_g	group velocity, m/s.
f	wave frequency, Hz.
$S(f)$	one-dimensional frequency spectrum, m^{2}s.
m_j	spectral moment of jth-order, m^2/s^j.
$F(\mathbf{k})$	two-dimensional wave number spectrum, m^4/rad^2.
a_n	amplitude of the nth-wave component, m.
φ_n	phase of the nth-wave component, rad.
$\mathbf{k}_n$	wave number vector of the nth-wave component, rad/m.
σ_η^2	variance of η, m^2.
$\zeta(\mathbf{r})$	complex signal, m.
$\eta(\mathbf{r})$	wave elevation over the mean sea level (real part of the complex signal), m.
$\hat{\eta}(\mathbf{r})$	imaginary part of the complex signal, m.
$G(\mathbf{r})$	group train, m^2.
$P(\mathbf{r})$	pulse train, m^2.
$E(\mathbf{r})$	two-dimensional SIWEH function, m^2.
GF	groupiness factor.
$\rho(\mathbf{r})$	wave envelope, m.
$\hat{\eta}_t(\mathbf{r})$	two-dimensional total Hilbert transform of $\eta(\mathbf{r})$, m.
$\rho_t(\mathbf{r})$	wave envelope estimation derived from total Hilbert transform, m.
$\tilde{\rho}_t(\mathbf{r})$	smoothed wave envelope estimation, m.
R_{mean}	mean run area, m^2.
R_{max}	area of the largest run, m^2.
γ	wave height correlation coefficient.
Q_p	peakedness factor.
ν	spectral bandwidth.
C_{lin}	degree of nonlinearity parameter for SAR imagery.

[38] **Acknowledgment.** This work has been carried out within the framework of the MaxWave project, which is partially funded by the European Commission (contract EVK:3-2000-00544).

References

Alpers, W., D. B. Ross, and C. L. Rufenach (1981), On the detectability of oceans surface waves by real and synthetic aperture radar, *J. Geophys. Res.*, *86*, 710–732.

Battjes, J. A., and G. P. van Vledder (1984), Verification of Kimura's theory for wave group statistics, paper presented at 19th Coastal Engineering Conference, Am. Soc. of Civ. Eng., Houston, Tex.

Breit, H., B. Schättler, and U. Steinbrecher (1997), A high precision workstation-based chirp scaling SAR processor, paper presented at IGARSS97 International Conference, Int. Geosci. and Remote Sens. Symp., Singapore.

Brüning, C., W. Alpers, and K. Hasselmann (1990), Monte-Carlo simulations studies of the nonlinear imaging of a two dimensional surface wave field by a synthetic aperture radar, *Int. J. Remote Sens.*, *11*(7), 1695–1727.

Bülow, T., and G. Sommer (2001), Hypercomlpex signals—A novel extension of the analytic signal to the multidimensional case, *IEEE Trans. Signal Process.*, *49*(11), 2844–2852.

Dankert, H., J. Horstmann, S. Lehner, and W. Rosenthal (2003), Detection of wave groups in SAR images and radar-image sequences, *IEEE Trans. Geosci. Remote Sens.*, *41*, 1437–1446.

Donelan, M. A., W. M. Drennan, and A. K. Magnusson (1996), Nonstationary analysis of the directional properties of propagating waves, *J. Phys. Oceanogr.*, *26*(9), 1901–1914.

Funke, E. R., and E. P. D. Mansard (1980), On the synthesis of realistic sea states, paper presented at 17th International Conference on Coastal Engineering, Am. Soc. of Civ. Eng., Sydney, N. S. W., Australia.

Goda, Y. (1970), Numerical experiment on wave statistics with spectral simulation, *Rep. Port Harbour Res. Inst.*, *9*(3), 3–57.

Goda, Y. (2000), *Random Seas and Design of Maritime Structures*, World Sci., River Edge, N. J.

Gran, S. (1992), *A Course in Ocean Engineering*, Elsevier Sci., New York.

Hamilton, J., W. H. Hui, and M. A. Donelan (1979), A statistical model for groupiness in wind waves, *J. Geophys. Res.*, *84*, 4875–4884.

Hasselmann, K., and S. Hasselmann (1991), On the nonlinear mapping of an ocean wave spectrum into a synthetic aperture radar image spectrum, *J. Geophys. Res.*, *96*, 10,713–10,729.

Hasselmann, K., R. K. Raney, W. J. Plant, W. Alpers, R. A. Shuchman, D. R. Lyzenga, C. L. Rufenach, and M. J. Tucker (1985), Theory of synthetic aperture radar ocean imaging: A MARSEN view, *J. Geophys. Res.*, *90*, 4659–4686.

Holland, K. T., R. A. Holman, T. C. Lippman, J. Stanley, and N. Plant (1997), Practical use of video imagery in nearshore oceanographic field studies, *IEEE J. Oceanic Eng.*, *22*(1), 81–92.

Kimura, A. (1980), Statistical properties of random wave groups, paper presented at 17th International Conference on Coastal Engineering, Am. Soc. of Civ. Eng., Sydney, N. S. W., Australia.

Komen, G. J., L. Cavaleri, M. A. Donelan, K. Hasselmann, S. Hasselmann, and P. A. E. M. Janssen (1994), *Dynamics and Modelling of Ocean Waves*, Cambridge Univ. Press, New York.

Krogstad, H. E. (1992), A simple derivation of Hasselmann's nonlinear ocean synthetic aperture radar transform, *J. Geophys. Res.*, *97*, 873–885.

Lehner, S., B. Schättler, J. Schulz-Stellenfleth, and H. Breit (1998), Processing and calibration of ERS SAR single look complex imagettes-extraction of wind and sea state parameters, paper presented at CEOS SAR Calibration and Validation Workshop '98, Comm. on Earth Obs. Satell., Noordwijk, Netherlands.

Lehner, S., J. Schulz-Stellenfleth, B. Schättler, H. Breit, and J. Horstmann (2000), Wind and wave measurements using complex ERS-2 SAR wave mode, *IEEE Trans. Geosci. Remote Sens.*, *38*, 2246–2257.

Longuet-Higgins, M. S. (1952), On the statistical distribution of the heights of sea waves, *J. Mar. Res.*, *11*, 245–266.

Longuet-Higgins, M. S. (1984), Statistical properties of wave groups in a random sea-state, *Philos. Trans. R. Soc. London, Ser. A*, *312*, 219–250.

Longuet-Higgins, M. S. (1986), Wave groups statistics, in *Oceanic Whitecaps*, edited by E. C. Monahan and G. M. Niocaill, D. Reidel, Norwell, Mass.

Medina, J. R., and R. T. Hudspeth (1990), A review of the analyses of ocean wave groups, *Coastal Eng.*, *14*, 515–542.

Nieto Borge, J. C., K. Reichert, and J. Dittmer (1999), Use of nautical radar as a wave monitoring instrument, *Coastal Eng.*, *37*, 331–342.

Nieto Borge, J. C., A. Niedermeier, S. Lehner, and W. Rosenthal (2003), Determination of wave field properties in the spatial domain from spaceborne SAR images, paper presented at 22nd International Conference on Offshore Mechanics and Arctic Engineering, Am. Soc. of Mech. Eng., Cancun, Mexico.

Ochi, M. K. (1998), *Ocean Waves: The Stochastic Approach*, Cambridge Univ. Press, New York.

Piotrowski, C. C., and J. P. Dugan (2002), Accuracy of bathymetry and current retrievals from airborne optical time-series imaging of shoaling waves, *IEEE Trans. Geosci. Remote Sens.*, *40*, 2606–2618.

Rice, S. O. (1945), Mathematical analysis of random noise, *Bell Syst. Tech. J.*, *23*, 282–332.

Rice, S. O. (1974), Wave group formation among storm waves, paper presented at 14th International Conference on Coastal Engineering, Am. Soc. of Civ. Eng., Copenhagen.

Schulz-Stellenfleth, J., and S. Lehner (2004), Measurement of two dimensional sea surface elevation fields using complex synthetic aperture radar data, *IEEE Trans. Geosci. Remote Sens.*, in press.

Sorensen, R. M. (1994), *Basic Wave Mechanics: For Coastal and Ocean Engineers*, John Wiley, New York.

Stark, H. (1971), An extension of the Hilbert transform product theorem, *Proc. IEEE*, *59*, 1359–1360.

Trulsen, K. (2000), Simulation the spacial evolution of a measured time series of a freak wave, paper presented at Workshop on Rogue Waves 2000, Inst. Fr. de Rech. pour l'Exploit. de la Mer, Brest, France.

Trulsen, K., and C. T. Stansberg (2001), Special evolution of water surface waves: Numerical simulation and experiment of bichromatic waves, paper presented at ISOPE'2001, Int. Soc. of Offshore and Polar Eng., Stavanger, Norway.

S. Lehner, A. Niedermeier, J. C. Nieto Borge, and J. Schulz-Stellenfleth, Remote Sensing Technology Institute (IMF), German Aerospace Center (DLR), Oberpfaffenhofen, Wessling D-82234, Germany. (susanne.lehner@dlr.de; andreas.niedermeier@dlr.de; jose.c.nieto@dlr.de; johannes.schulz-stellenfleth@dlr.de)